Northumbria University
NEWCASTLE

Arc Ablation Behavior and Microstructure Evolution of Plastically Deformed and Micro-alloyed Cu-Cr-Zr Alloys

Kai Zhou[1], Wenge Chen[1*], Pei Feng[1], Fanglong Yan[1], Yongqing Fu[2*]

[1] School of Materials Science and Engineering, Xi'an University of Technology, Xi'an, Shaanxi, 710048, P.R. China

[2] Faculty of Engineering and Environment, Northumbria University, Newcastle upon Tyne, NE1 8ST, UK

Abstract: Cu-Cr-Zr alloys are often subjected to premature failures due to arc erosion at moment of their breakdown. In this paper, a series of simulated high-voltage arc ablation experiments were conducted to systematically investigate arc ablation characteristics of Cu-Cr-Zr alloys, their microstructure evolutions and anti-ablation properties after plastic deformation and microalloying. Results showed that during their arc ablation processes, a halo pattern was firstly formed on the surface under the action of high-temperature arc. This is followed by partial melting and splashing of Cu, forming of uneven and rough surfaces, and finally significant burning of the alloy. The degree of ablation of alloy is aggravated with the increased breakdown voltage. Due to a combined effect of solid solution strengthening, fine grain strengthening and deformation strengthening, the ablation resistance of the micro-alloyed and plastically deformed alloy has been significantly improved. The breakdown field strengths of commercial Cu-Cr-Zr alloy, heat-treated and deformed one, micro-alloyed and heat-treated one are 1.46×10^6 V/m, 1.67×10^6 V/m and 1.90×10^6 V/m, respectively. However, the breakdown strength of alloys after microalloying is unstable. Results show that there are no preferred phases formed after the first breakdown of arc ablation of Cu-Cr-Zr alloys. The second-phase particles with high-hardness and high-melting temperature hinder the splashing and flow of the molten copper, and inhibit the movement of the cathode spots during the ablation process.

Keywords: Cu-Cr-Zr alloy; Arc ablation; Microstructure; Ablation mechanism

1 Introduction

Cu-Cr-Zr alloys have many outstanding properties such as high strength, good electrical

[1] Corresponding authors: Professor Wenge Chen; Prof. Richard Y.Q.Fu.
E-mail: wgchen001@263.net (W.G. Chen), richard.fu@northumbria.ac.uk (Richard Y.Q. Fu)

conductivity, good plasticity and thermal conductivity, therefore, they have been widely used as electric slide materials, spot welding electrodes and electrical contact materials [1-5]. However, it is a challenge to improve both the electrical properties and mechanical properties of the Cu-Cr-Zr alloys. To solve this problem, various methods such as micro-alloying, plastic deformation and heat-treatment have been used to enhance the properties of the Cu-Cr-Zr alloys. For examples, it was reported that introducing the third alloying components such as Zr [6], Fe [7], Mg [8] into the CuCr alloys could improve their overall properties. Pang et al. [6] studied the effect of Zr and (Ni, Si) additions into the Cu-Cr alloys for the improvement of their mechanical and electrical properties, and reported that the increased hardness and electrical conductivity of the alloys are 177 HV and 82.2% IACS (International Annealing Copper Standard). Zhao et al. [8] added Mg element into CuCr alloys using a melting method, and found that the tensile strength and electrical conductivity were 540 MPa and 79.2% IACS after heat-treatment. Li et al. [9] used a two-step cryo-rolling and aging treatment to fabricate Cu-Cr-Zr alloy, and achieved an ultimate tensile strength of 648 MPa and electrical conductivity of 79.80% IACS. Kulczyk et.al. [10] fabricated Cu-Cr-Zr alloys using several cold working and ageing treatment, and obtained ultrafine-grained structure with a high tensile strength of 630 MPa and an electrical conductivity of 78% IACS. Mishnev et al. [11] used a multiple equal channel angular pressing method at 473-673 K to prepare the Cu-Cr-Zr alloys, and they obtained a high yield strength of 535 MPa and small reductions in electrical conductivity from 80%IACS to 70%IACS.

To the best of our knowledge, there are no reports on the studies of arc ablation behavior of Cu-Cr-Zr alloys, and the current research on the anti-ablation properties are mainly focused in pseudo Cu-based alloys such as CuZr [12], WCu [13,14] and CuCr [15-17]. Li et al. [12] investigated air anti-erosion properties. They reported the significant mass loss and changes of morphology after 10,000 discharge cycles, and also found that the $ZnSnO_4$ phase can enhance the oxidation resistance at a high temperature. Dong et al. [13] used an arc polarization process to investigate the ablation morphology and mechanism of graphene-doped WCu composites using an operation voltage of 10 kV. Yang et al. [15] prepared nanocrystalline CuCr5 alloy using a single-roller melt spinning method. They found that the arcs were more stable at nano-scale grains, and their chopping currents were lower than those on the coarse grains. Cao et al. [16] found that the addition of Mo in CuCr alloys can strengthen the Cr phase, and the first breakdown phase was changed from Cr phase to Cu phase. Meanwhile, addition of Mo can also improve arc stability and reduce concentrated ablation pits.

In order to systemically study the arc erosion properties of Cu-Cr-Zr alloys, an arc ablation simulation experiment is firstly applied to the Cu-Cr-Zr alloys in this paper, and the anti-ablation performance of Cu-Cr-Zr alloys is studied with different treatment methods at different voltages. This study will clarify if there is any selective breakdown of alloy material (e.g., to check if there are simultaneous ablation of different components or ablation of low melting point components), and provide arc ablation mechanism and prevention solution for the Cu-Cr-Zr alloys.

2 Experimental method and materials

The material used in this work was a commercial Cu-Cr-Zr alloy (with its composition listed in Table 1). The heat treated and deformed sample of the commercial Cu-Cr-Zr was used, and was heat treated with solid-solution (at 960 °C for 1h) and aging (at 450 °C for 5h) processes. The severe plastic deformation tests were performed on the pre-cleaned samples using small energy multiple loading cyclic deformation at room temperature with a drop hammer impact tester. The energy of drop hammer impact was 4 J, and the period was 6 times/min. The deformation strain can be up to 90%. The micro-alloyed and heat-treated samples (commercial Cu-Cr-Zr alloys doped with 2.0 wt.% Ni, 0.3 wt.% La) were prepared using a vacuum arc melting method (SKY/DHL-400) under an argon atmosphere. After cooling down, alloy ingots of size 20mm × 10mm × 80mm were prepared, and heat treatment was performed, including solid solution process at 960 °C for 1h and aging at 450 °C for 5h. The properties of the materials under different treatments are summarized in Table 2.

Table 1 The main composition of commercial Cu-Cr-Zr alloy

Elements	Cr	Zr	Al	Mg	Fe	Si	P	Cu
wt.%	0.65	0.15	0.1-0.25	0.1-0.25	0.05	0.05	0.01	Bal.

Table 2 Hardness and conductivity of Cu-Cr-Zr alloy using different method of treatment

Properties	Commercial	Heat treated and deformation	Microalloying and heat treated
Hardness/HV	181	232	223
Conductivity/%IACS	81.1	73	67

Fig. 1 is a schematic illustration of experimental set-up for electric breakdown. After removing the surface stains by mechanical polishing and ultrasonic cleaning, the sample was used as cathode, and a pure W needle electrode was used as the anode. Under a vacuum of 10 Pa, the voltage was adjusted to 8 kV and 16 kV, and the W electrode was slowly moved toward the sample surface with a speed of 0.01 mm/s. When the distance between the tip of the electrode and the sample surface is sufficiently small, the anode and cathode will generate an arc discharge under the large voltage. The breakdown voltage and distance at the time of discharge were immediately recorded, and the breakdown field strength was calculated according to Eq.1. Each test was repeated for 100 times. The mass of samples was weighed to obtain a weight loss curve. Detailed morphological characteristics of the Cu-Cr-Zr alloys were obtained using a transmission electron microscope (TEM, JEM-3010, JEOL, Japan). Surface morphologies of samples after arc breakdown were observed using a scanning electron microscope (SEM, JSM-6700E) with an energy dispersion spectrometer (EDS).

$$E_i = \frac{U_i}{d_i} \quad \text{(Eq.1)}$$

in which *U* is the breakdown voltage, *d* is the breakdown distance, *E* is the dielectric strength, and *i* is the number of times.

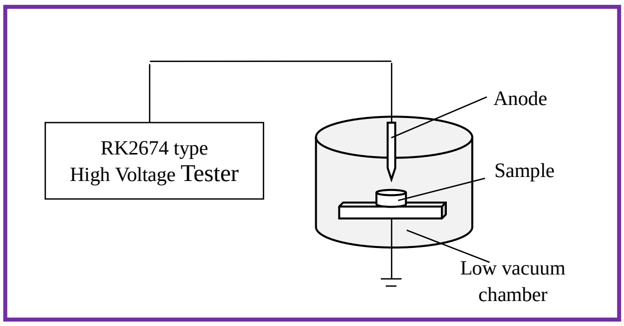

Fig. 1 The schematic of experimental device of electric breakdown

3 Results and discussion

3.1 Microstructure and morphology of Cu-Cr-Zr alloy after different treatments

Fig. 2 shows the microstructure of Cu-Cr-Zr alloy after different treatments. The commercial alloy has a uniform grain size and clear grain boundaries, and there are many white precipitates. From the phase diagram [18] and EDS analysis, the white precipitates are Cu_4Cr (see Fig. 2a). In order to observe the distribution of the precipitates in the matrix, TEM analysis was performed and the results are shown in Fig. 2b. The precipitates are confirmed to be Cr particles, and the secondary phase of Cr is dispersed uniformly in the Cu matrix, which is similar to those reported in literature [19]. As shown in Fig. 2c, for the alloy after the heat treatment and deformation, precipitates of secondary phase (e.g., many circular or worm-like ones) are existed in matrix after plastic deformation. The structures are formed into parallel and thin deformed bands under severe plastic deformation, with their thickness of about a few microns. The degree of deformation of each grain is different due to their different orientations, and their slip systems and the angle of the deformation directions are different. The number of crystal boundaries are increased and the secondary phases appear to be existed in the boundary position. TEM image of the Cu-Cr-Zr alloy after the heat treatment and deformation is shown in Fig. 4d, which shows the existence of larger Cr particle and smaller Zr dispersion phases in the precipitates. The remaining gray-white substance is the copper substrate. After micro-alloying and solid-dissolved aging treatment, the substrate surface shows small spherical black particles and small white particles as shown in Fig. 2e. From the EDS analysis, these small black particles contain Cu, Zr, Ni elements, and white particles only contain Cu and Ni elements. Fig. 2f shows the TEM image of micro-alloying and heat-treated Cu-Cr-Zr alloys, and the precipitates contains Cr and Zr phases.

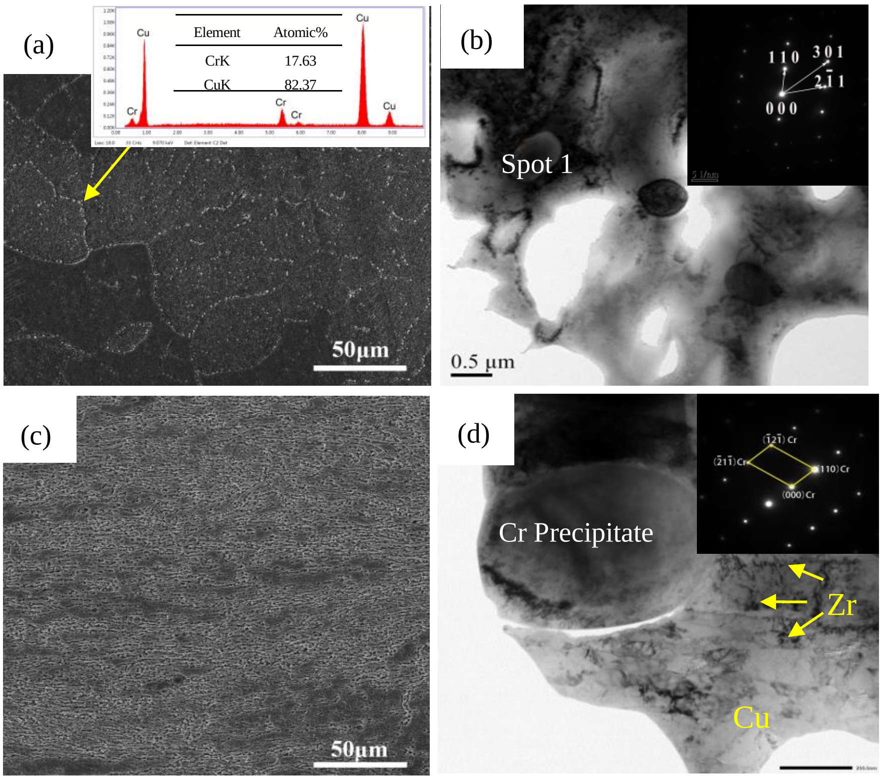

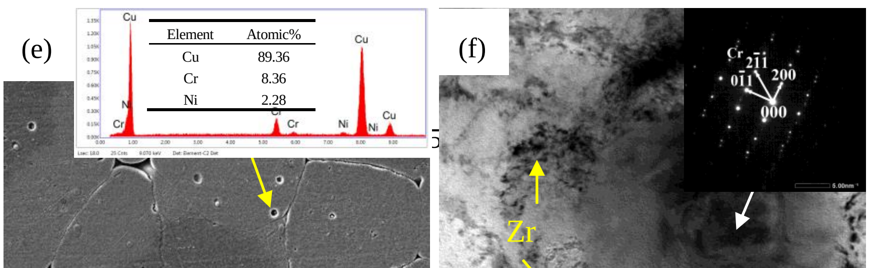

Fig. 2. Microstructure morphology of Cu-Cr-Zr alloys with different treatment: (a) The SEM image of commercial alloys; (b) The TEM image of commercial alloys; (c)The SEM image after heat treatment and deformation; (d)The TEM image after heat treatment and deformation; (e)The SEM image after micro-alloying + heat treatment; (f)The TEM image after micro-alloying and heat treatment

3.2 Arc erosion weight loss of Cu-Cr-Zr alloy with different treatments

The results of arc breakdown times and weight loss of Cu-Cr-Zr alloys with 8 kV and 16 kV under arc erosion processes are plotted in Fig. 3. The accumulated weight loss is increased with the increasing of breakdown times. For the same treated samples, the arc ablation weight loss is more serious at a higher voltage level, however, the increase rate of different samples is different. The weight changes of those samples after micro-alloying are more obvious, whereas those after heat treatment and serious plastic deformation show only a little changes. This is related to the overall performance of conductivity and strength of the alloys after the different treatments (see Table 2).

An amount of ablation is increased with the number of breakdowns. Because there are microscopic sharp edges and burrs of the sample at the sample surface, there will be strong electron and ion charging effects generated at those spots. These places will result in intense heating and ion sputtering, thus resulting in the rapid removal of sharp edges, burrs, and oxides from the surface. Due to the arc of the breakdown accompanied by the burning of the material, a significant weight loss has occurred. After a certain number of breakdowns, the melted splash and cooling solidification of copper reach a dynamic equilibrium. With the increase in the number of breakdowns, Cu droplets are further sputtered away, and the specimen surface becomes uneven and rough, so that the amount of ablation of the specimen will be increased rapidly. The more the breakdowns happening, the more obvious the phenomenon of rough surface. There are three stages, e.g., initial phase, stable intermediate stage and late stage of ablation failure experienced by contact arc ablation, which has been reported in literature [19, 22]. However, we can only see two obvious stages in Fig. 3, e.g., the initial stage within the first

30 cycles and the stable ablation stage based on the slope changes. The Cu-Cr-Zr alloys can reach the stable stage with much less cycles, the reasons are their lower hardness, good conductivity and the easy breakdown of electron. The third stage of rapid failure cannot be observed clearly in Fig. 3, probably because there needs a long-term equilibrium process between copper sputtering, evaporation and solidification and the Cu content of Cu-Cr-Zr alloys is more than that in pseudo alloys such as tungsten copper or chromium copper.

The stable stage of the Cu-Cr-Zr alloy after the heat treatment and deformation (see Fig. 3b) is much longer, mainly because the hard second-phase particles generated during the heat treatment process are more evenly distributed and precipitated. During the subsequent deformation process, great amount of crystal boundaries are generated, forming more uniform distribution and non-deformable second-phase particles. The mechanical properties of alloys are enhanced significantly due to deformation reinforcement, solid-soluble reinforcement and dispersion-reinforced effects. However, these reinforcement methods could influence the electrical properties of the alloys (see Table 2). The electrical conductivity was reduced, mainly because the electrons are scattered by many secondary particles. Meanwhile, the spots are moved from one site to next site through deflection and jumping rather than smoothly moving, thus resulting in the slightly improved arc corrosion performance. From above analysis, in order to achieve low voltage and ultra-high arc discharge cycles for the CuZr [12] or CuCr [17] alloys, the problem of arc erosion can be solved using the method which can produce uniform dispersed secondary particles in Cu-Cr-Zr alloys.

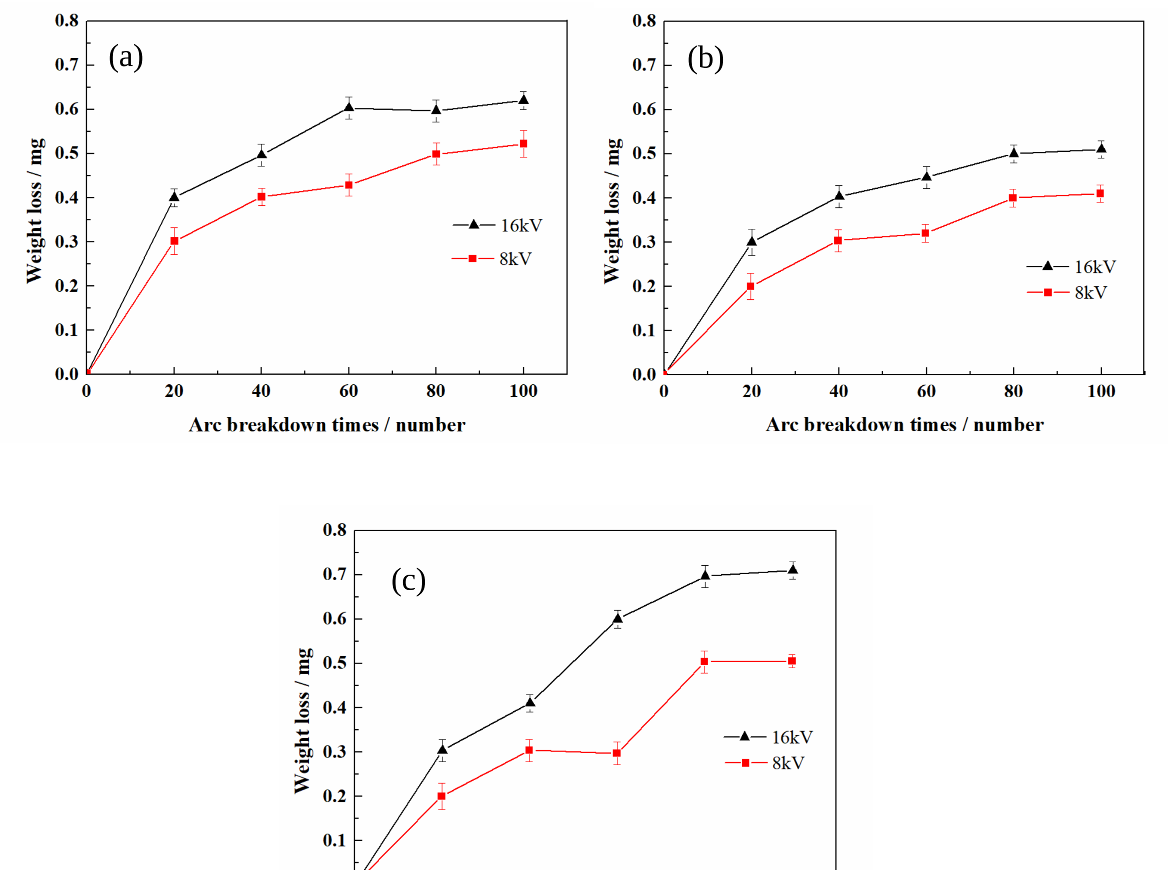

Fig. 3 The curves of arc erosion weight loss of Cu-Cr-Zr alloy in different treatment

(a) Commercial; (b)Heat treated and deformation; (c) Micro-alloyed and heat treated

3.3 Erosion morphologies after the first arc breakdown

Fig. 4 shows SEM images after the first arc erosion for the samples of commercial, heat treated and deformed, micro-alloyed and heat-treated Cu-Cr-Zr alloys. The ablation spots (also called cathode spots or ablation pits) of the first arc show an approximately circular halo (as indicated by the arrow in the Fig. 4) after each treatment, which is similar to the first breakdown phenomenon happened in the pure Cu [21]. The ablation halo and the ablation pit are circular. The ablation pit of Cu-Cr-Zr alloy has a smaller melted area, because the addition of hard precipitates hinders the heat conduction though the copper alloy. The colors of middle and surrounding area are much darker, and the secondary circle and the outermost color become much brighter as shown in Figs. 4a, 4c and 4e. There is a certain distance between the two heat arc impact zones, indicating that the spot motion has shown a jumping pattern. The velocity of motion is approximately 15-25 m/s, which is similar with that reported in the Ref [15]. Furthermore, Cu-Cr-Zr alloys after the different treatments have different first breakdown spots, and the number of spots in commercial alloy is reduced (see Fig. 4a). The white arrows indicate jumping paths of the arc, and the alloy with micro-alloying and plastic deformation shows several obvious ablation spots (see Figs. 4c and 4e). Results show that the alloy after plastic deformation and micro-alloying has an ability to disperse the arc, thus its resistance to arc erosion has been improved.

To illustrate the composition of the ablation pit after the first breakdown, EDS spectrum analysis was performed on the first breakdown center of the alloy at three different points for each sample. The center of the ablation pit and the convex part are mainly copper. In addition, a small amount of chromium and zirconium in the form of a secondary phase are existed in the compound. Although a trace amount of nickel is existed in the micro-alloyed sample, the composition of these spots is basically the same, indicating that the first breakdown of the alloy surface is non-selective. This is different from that described in the literature [22,23], because the Cu-Cr-Zr alloy in this work satisfy the condition of ternary phase diagrams. There are no obviously low work function phases which are preferred to generate arcing.

The ablation pit in the alloy with heat-treatment and deformation processes (Fig. 4c) is different from the erosion phenomenon observed in the other samples. An enlarged image (embedded diagram in Fig. 4c) shows that it has a typical layered structure, which is generated in the process of the small energy multi-shock deformation. The arc energy is concentrated here as there are cracks, which causes intense ablation. This local surface of the alloy is melted, sputtered and then cracked. The EDS spectrum analysis of the point 1 in the Fig. 4(c) shows that it is the secondary phase of copper zirconium.

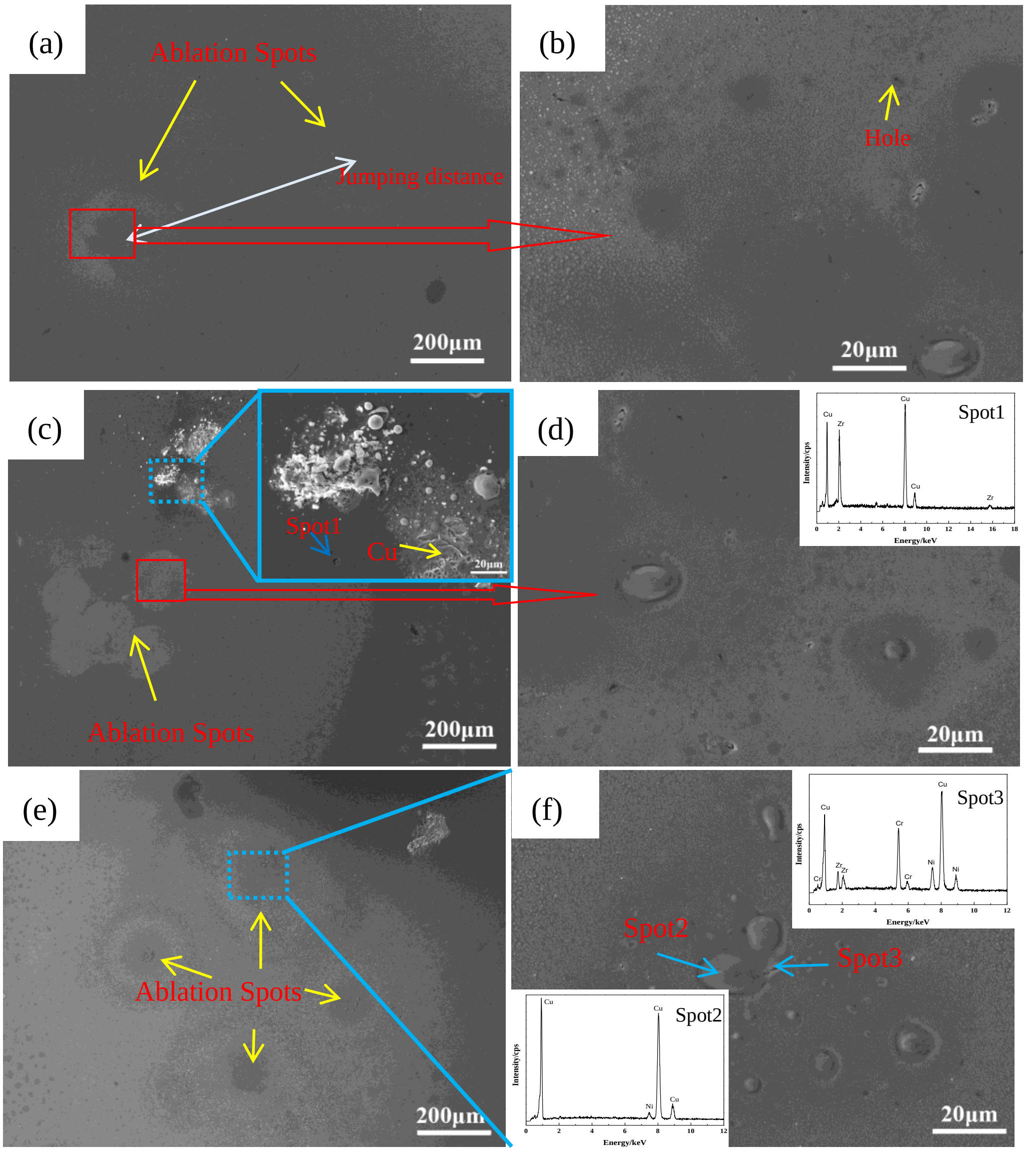

Fig. 4 The erosion morphologies of Cu-Cr-Zr alloys after first arc breakdown: (a, b) Commercial alloy; (c, d) Heat treated and deformation alloy; (e, f) Micro-alloying and heat treated; insets are the EDS spectrum of spots 1, 2, 3, respectively

3.4 Morphologies of Cu-Cr-Zr alloys after 100 times arc erosion under different voltages

Figs. 5-7 are the SEM images of Cu-Cr-Zr alloys with different treatments, after 100 times electrical breakdown at different voltage levels. In these figures, we can see that during the arc ablation process, pits and protrusions of different sizes are distributed on the ablated surfaces. At a low magnification (Fig. 5a), it is apparent that the low melting point component of the alloy material melts under the action of heat, and the remaining pores can be seen at a high magnification (Fig. 5b). The low melting point component of Cu is evaporated, thus causing the formation of irregular protrusions after vaporization and sputtering of the Cu. As reported in the literature [21], it is believed that when the current is applied, more electrons and ions are generated due to collision of electrons with gas medium molecules. In this process, the numbers of electrons and ions are increased drastically, and a discharge channel is formed in the medium, thus generating the arc ablation. When the electric field strength in the circuit exceeds the arcing limit of the sample, severe arc ablation occurs on the surface of the sample. The low melting point component of the sample is melted, vaporized and splashed. Meanwhile, part of the secondary phases with a high melting point is also melted. It can be seen from Figs. 5a and 5c that the area of ablation is increased with the increase of voltage level. Similar trends can be found for the phenomena of sputtering of copper, irregular protrusions, and the breakdown voltage. Meanwhile the low-melting Cu phase is splashed due to of high energy density, resulting in the phenomena of droplets and caters on surface. The arc energy is applied to the much deeper layer during further ablation. It can be seen from Figs. 5b and 5d that the molten surface is more obvious under a high breakdown voltage, and there is obvious ablation hole as shown by the red arrow in Figs. 5d and 6d.

Fig. 6a shows droplets having a large surface and a relatively uniform distribution, with an average diameter of about 5 μm. When the breakdown voltage is increased up to 16 kV, the droplet in the ablation pit becomes irregular shapes and have a diameter of about 10 μm, with much smaller ablation pits. In Fig. 7, after 100 breakdown times, the surface of the alloy shows a significant ablation phenomenon, and the ablation pit is large and shallow. EDS analysis of the arrow position in Fig. 7a shows that the surface of the ablation pit is mainly the copper phase condensed on the ablated region after splashing. Small amounts of Ni and La are observed, indicating that the compounds are formed in the material. As reported in literature [23-25], the refined grains can result in the increase of grain boundaries, and provide conditions for electron emission. The ablation resistance of alloys is improved because the cathode spots have been moved continuously. However, after each breakdown process, micro-protrusions are generated and become easy-arcing positions in the subsequent breakdown [26], and finally form the microscopic topography as shown in Fig. 7b.

A comparison was made between Cu-Cr-Zr alloys after different treatments using the same breakdown voltage after 100 breakdown times. When the breakdown voltage is 8 kV, the plastically deformed alloy (see Fig. 6a) shows surface with a smaller droplet diameter and a shallower ablation depth than those of the undeformed alloys. Because the grain is small after plastic deformation, the precipitated phase is more evenly distributed in the copper matrix. There are many new grain boundaries formed, which make the breakdown more uniform, as those reported in Ref [26]. After the ablation, the alloy with heat-treatment and microalloying shows a large extent of erosion on the surface, and the surface protrusions are irregular and uneven.

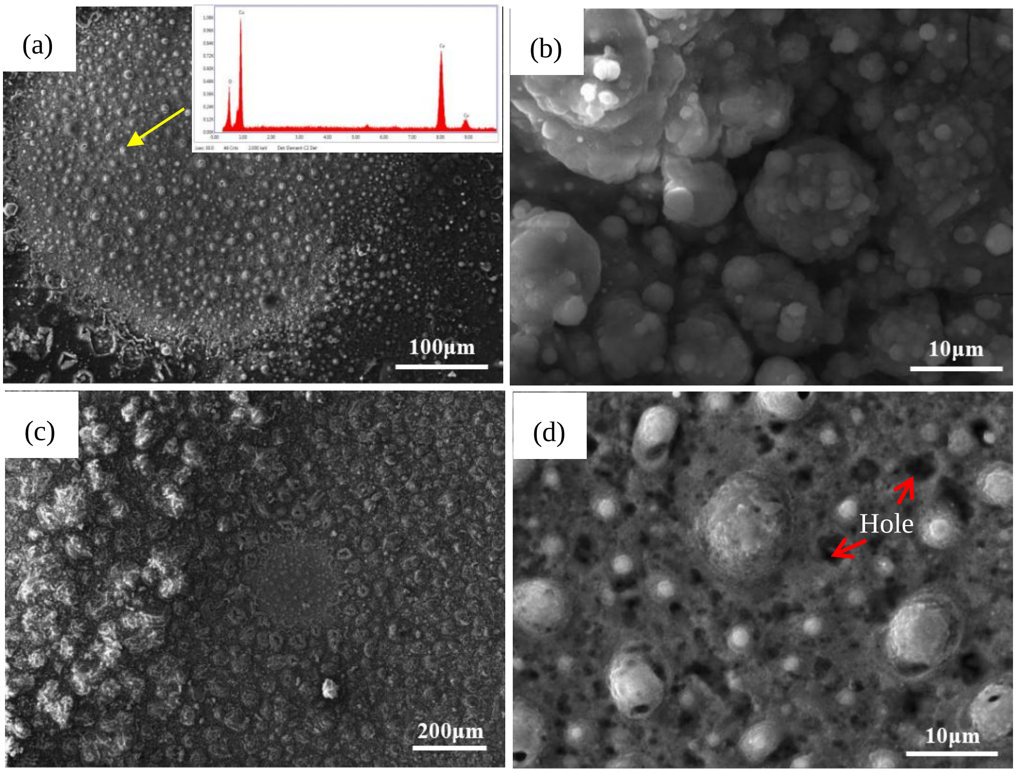

Fig. 5 SEM micrographs of commercial Cu-Cr-Zr alloys after 100 breakdown times under different voltage levels: (a) (b) 8kV; (c) (d) 16kV

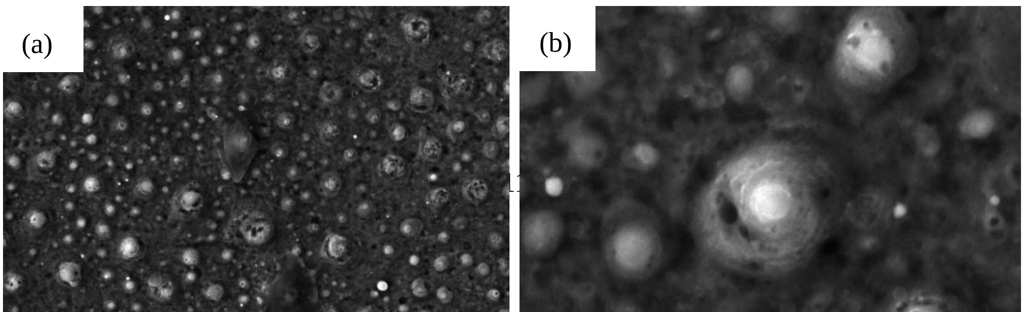

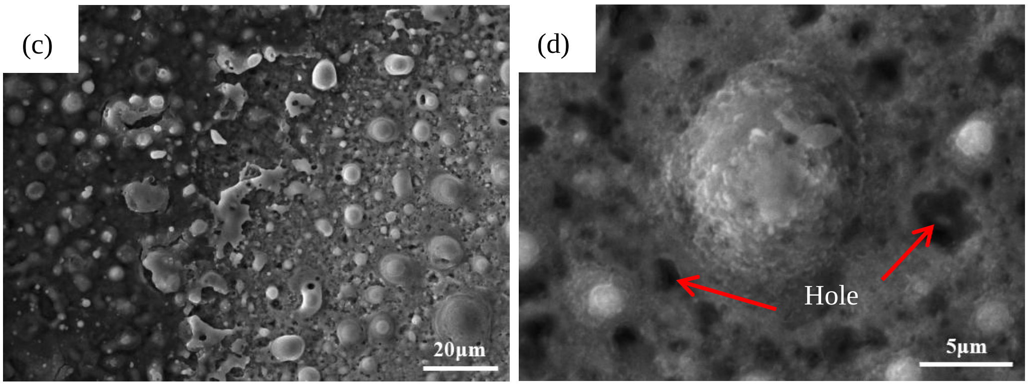

Fig. 6 The SEM micrographs of Cu-Cr-Zr alloys with heat-treated and deformation after 100 breakdown times under different voltage levels

(a) (b) 8kV;(c) (d) 16kV

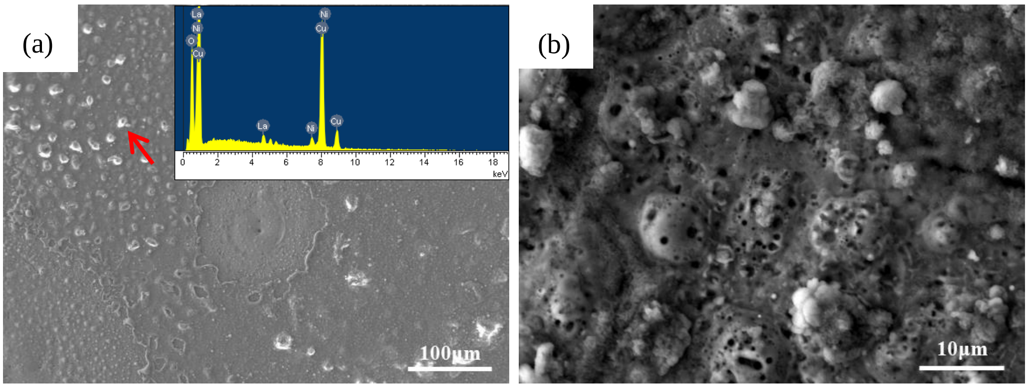

Fig. 7 The SEM micrographs of Cu-Cr-Zr alloys with micro-alloying and heat-treated after 100 breakdown times under 8kV

3.5 Anti-ablation properties of Cu-Cr-Zr alloys

Figure 8 shows relationships between dielectric strength and number of breakdown times, and the statistical distribution of breakdown of different Cu-Cr-Zr alloys. In Fig. 8a, the dielectric strength is approximately 1.46×10^6 V/m. When the voltage is increased to 16 kV, the dielectric strength fluctuates within a certain range and its distribution is scattered as shown in Fig. 8b. However, the average dielectric strength is about 1.43×10^6 V/m, which is slightly lower than that at 8 kV. During the 100-time breakdown of the heat treated and deformed alloy (Fig.8 c, d), the dielectric strength of the alloy under 8 kV shows a stable trend, and the average field strength is 1.57×10^6 V/m. The dielectric strength distribution of the alloy under 16 kV is scattered, with an average value around 1.67×10^6 V/m. It can be seen from Fig. 8e that the alloy of micro-alloyed and heat-treated has a large increase in the breakdown field strength compared with the alloy without adding the rare earth elements. This is because the distribution of secondary phase containing Cr and Zr is more uniform compared with those without adding the rare earth element, although its dielectric strength (see Fig.8e) shows serious fluctuation.

It can be concluded that as the external voltage level increases, the fluctuation of the breakdown field strength increases. The reason is attributed to the high arc energy during breakdown at higher voltages. The higher the arc energy during each breakdown, the larger the surface roughness of the alloy compared to the low voltage level (shown in the above 100 breakdown micrographs). Therefore, the arc will firstly occur at protrusion, causing the field strength significantly fluctuated. When the voltage is 8 kV, the alloy of heat treated and deformed show the improved arc erosion resistance compared with that of the commercial one, and the breakdown field strength fluctuation is also reduced. The reason is that the number of grain boundaries is further increased during the deformation process, and the material is more evenly distributed.

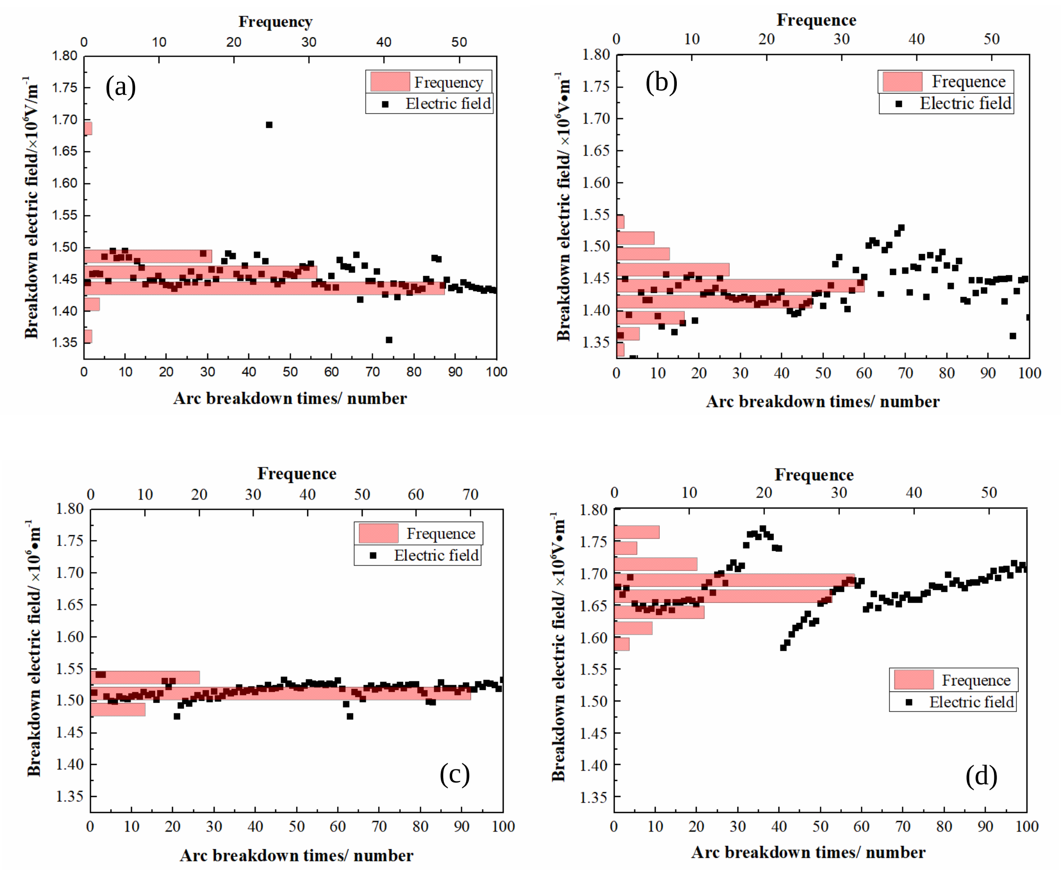

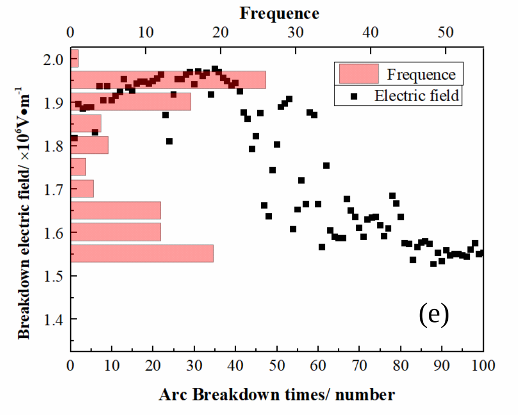

Fig. 8 Relationships between dielectric strength and number of breakdown statistical distribution of breakdown of Cu-Cr-Zr alloys: (a) Commercial alloys 8kV; (b) Commercial alloys 16kV; (c)Heat-treated and deformation 8kV; (d) Heat-treated and deformation 16kV; (e)Microalloying and Heat-treaded 8kV

4 Investigation on mechanism of arc erosion

The arc ablation behavior of Cu-Cr-Zr alloys has influences on the properties of the alloy applied in the process of power transmission. The physical properties of the material, such as microstructure, processing state, and heat conduction influence the arc ablation characteristics. In this paper, Cu-Cr-Zr alloys have applied with different processes such as heat treatment, plastic deformation and microalloying. After the heat treatment, the secondary phase was uniformly precipitated [27] and solid solution strengthening is achieved. However, the increase of defects such as lattice distortion, dislocations, and impurities in the alloys will prevent the transfer of electrons in the material. The plastic deformation and alloying can change the distribution of secondary phases in the material, resulting in the refined grains. The internal grain size of the alloy is decreased, and the numbers of grain boundaries are increased sharply. The precipitated phases are accumulated at the grain boundary, which increases the energy at the grain boundary [28]. The mobilities of electrons are low, so that the arc spots are jumping to other sites rather than smooth moving. The arc ablation resistance of alloys is improved because the arc energy has further been dispersed.

The outer electrons will escape from the alloys surface under an electric field, so that the electron density between the anode and the cathode is greatly increased. When the electric field intensity reaches the critical field emission density [26], the arc breakdown occurs. Then, the cathode spot moves to surrounding area randomly, and the motion direction of spots will change or jump when spots is hindered by the secondary phases (due to their high hardness and high melting point), as depicted with the yellow arrows in Figs. 9b and 9d. The energy of arc is weakened in this process. However, the secondary phase can cause lattice distortion [29] of matrix, and the electron will be emitted due to the larger energy of distortion. In addition, the spots are constantly scattered until extinguished. However, the ablation area enlarges and extends to the inner of alloys with the increase of breakdown times, and the molten pool is continued to expand. The molten copper is sputtered by the electromagnetic force, forming craters and pits on the surface of the material. The arcing erosion becomes serious, and alloys forms the different morphologies as shown in Figs. 9c and 9e. This is consistent with the morphologies of alloys after 100 times breakdowns.

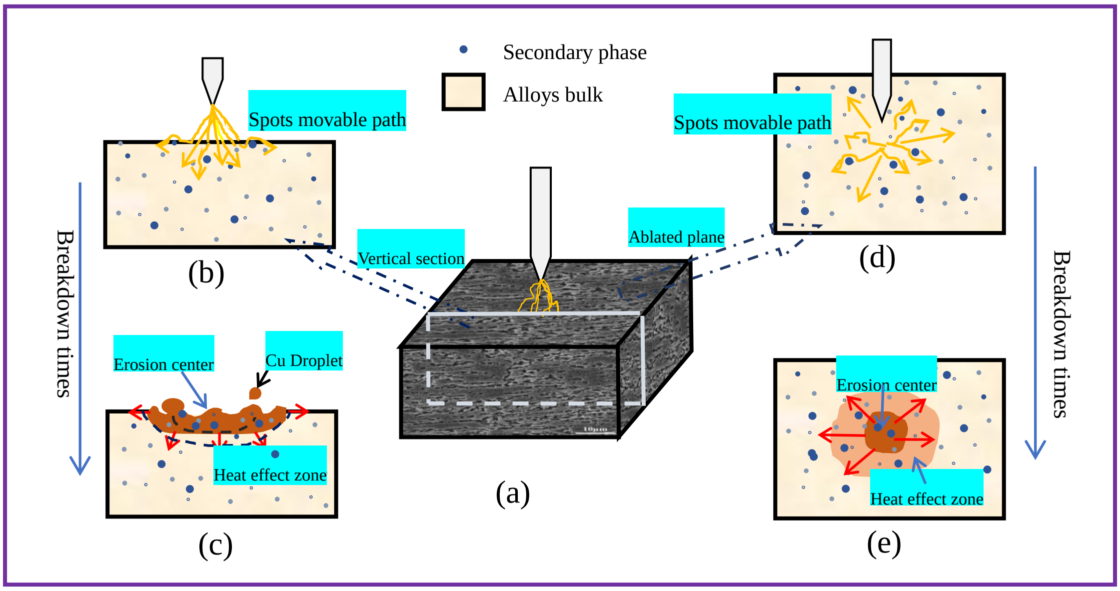

Fig. 9. Schematic representation of Cu-Cr-Zr alloys arc breakdown: (a) Macroscopic in ablation; (b) The movement of cathode spot in longitudinal section; (c) The morphology of sectional after breakdown; (d) The movement of cathode spot in ablative plane; (e) The morphology of surface ablation

5 Conclusion

(1) The mechanism of arc ablation of Cu-Cr-Zr alloy was proposed. It is considered that the first breakdown is non-selective and forms halo in the surface. Due to the dispersion of secondary phase, the cathode spots expand to the surrounding area by the form of jumping. In addition, the energy of arc will be decreased at the grain boundary or the secondary phase. The velocity of spots is 15-25m/s. After repeated ablation, there is a dynamic balance between the splashing of low-melting copper and cooling solidification, resulting in an uneven surface of the material. After the heat treatment, microalloying and deformation, there are effects of solid solution strengthening, fine grain strengthening, precipitation strengthening and deformation strengthening, therefore, more grain boundaries and secondary phases inhibit the movement and sputtering of spots, and these improve the properties of resistance to ablation.

(2) The weight loss of Cu-Cr-Zr alloy during ablation increases with increasing breakdown times and voltage. After 90% plastic deformation, the alloy has a weight loss of only 0.42 mg under 8 kV, dielectric strength of 1.67×10^{6} V/m with a minimum fluctuation.

Acknowledgements

The authors would like to acknowledge the financial supports from Xi'an Science research project of China (No.2017080CG/RC043) and Electrical Materials and Infiltration Key Laboratory of Shaanxi Province Projects (No.17JS080), Newton Mobility Grant (IE161019) through Royal Society and the National Natural Science Foundation of China, and Royal academy of Engineering UK-Research Exchange with China and India.

Reference

[1] J.Y. Cheng, B. Sheng, F.X. Yu. Precipitation in a Cu-Cr-Zr-Mg alloy during aging. Mater. Chcract. 81(4) (2013) 68-73.

[2] I.S. Batra, G.K. Dey, U.D. Kulkarni, et.al. Precipitation in a Cu-Cr-Zr alloy. Mater. Sci. Eng. A. 356 (1-2) (2013) 32-36.

[3] Q. Liu, X. Zhang, Y. Ge, et.al. Effect of processing and heat treatment on behavior of Cu-Cr-Zr alloys to railway contact wire. Metall Mater Trans A. 37(2006) 3233-8.

[4] A. Vinogradova, V. Patlanb, Y. Suzukib. Structure and properties of ultra-fine grain Cu-Cr-Zr alloy produced by equal-channel angular pressing. Acta Mater. 50(7) (2002) 1639-1651.

[5] M. Kulczyk, W. Pachla, J. Godek, et.al. Imoroved compromise between the electrical conductivity and hardness of the thermo-mechanically treared CuCrZr alloy. Mater. Sci. Eng. A. 724 (2018) 45-52

[6] Y. Pang, C. Xia, M. Wang, et.al. Effects of Zr and (Ni, Si) additions on properties and microstructure of Cu–Cr alloy. J. Alloys Compd., 582 (2014), pp. 786-792

[7] H. Fernee, J. Nairn, A. Atrens, Precipitation hardening of Cu-Fe-Cr alloys part I mechanical and electrical properties, J. Mater. Sci. 36 (2001) 2711-2719.

[8] Z.Q. Zhao, Z. Xiao. Z. Li, et.al. Effect of magnesium on microstructure and properties of Cu-Cr alloy. J. Alloys. Compd. 752 (2018)191-197.

[9] R.G. Li, E.Y. Guo, Z.N. Chen, et.al. Optimization of the balance between high strength and high electrical conductivity in CuCrZr alloys through two-step cryorolling and aging. J. Alloy. Compd. 771 (2019) 1044-1051.

[10] M. Kulczyk, W. Pachla, J. Gaodek, et.al. Improved compromise between the electrical conductivity and hardness of the thermo-mechanically treated CuCrZr alloy. Mater. Sci. Eng. A. 724 (2018) 45-52.

[11] R. Mishnev, I. Shakhova, A. Belyakov, et al. Deformation microstructures, strengthening mechanisms, and electrical conductivity in a Cu–Cr–Zr alloy. Mater. Sci. Eng. A. 629 (2015) 29-40.

[12] W.J. Li, W.Z. Shao, N. Xie, et.al. Air arc erosion behavior of CuZr/Zn2SnO4 electrical contact materials. J. Alloy. Compd. 743(2018) 697-706.

[13] L.L. Dong, W.G. Chen, N. Deng, et.al. Investigation on arc erosion behaviors and mechanism of W70Cu30 electrical contact materials adding graphene. J. Alloy. Compd.

696 (2017) 923-930.
[14]Q. Zhang, S.H. Liang, X.H. Yang, et.al. Failure analysis of CuW/CuCrZr contact materials in capacitor bank switch. Eng. Fail. Anal. 62 (2016) 156-163.
[15]Z.M. Yang, Q.L. Zhang, Q.F. Wang, et.al. Vacuum arc characteristics on nanocrystalline CuCr alloys. Vacuum. 81 (2006) 545-549.
[16]W.C. Cao, S.H. Liang, Z. Xiao, et.al. Effect of Mo addition on microstructure and vacuum arc characteristics of CuCr50 alloy. Vacuum. 85 (2011) 943-948.
[17]S.X. Zhu, Y. Liu, B.H. Tian, et.al. Arc erosion behavior and mechanism of Cu/Cr20 electrical contact material. Vacuum. 143(2017) 129-137.
[18]F.X. Huang, J.S. Ma, H.L. Ning, et.al. Analysis of phases in a Cu–Cr–Zr alloy. Scripta Mater. 48 (2003) 97-102.
[19]I. S. Batra, G. K. Dey, U. D. Kulkarni, et al. Microstructure and properties of a Cu-Cr-Zr alloy. J. Nucl. Mater. 299 (2001) 91-100.
[20]W.G. Chen, K. Zhang, B.J. Ding. A study on electric-lifetime of W-Cu contacts materials. Powder Metallurgy Technology. 4 (2003) 224-227.
[21]L.J. Wang, W.G. Chen. Effect of surface roughness on arc-erosion resistance of W-Cu alloy. Materials Science and Engineering of Powder Metallurgy. 21 (2016) 802-808.
[22]X.H. Yang, S.H. Liang, X.H. Wang, et.al. Effect of WC and CeO2 on microstructure and properties of W-Cu electrical contact material, Int. J. Refract. Met. Hard Mater. 28 (2010) 305-311.
[23]W.G. Chen, Z.Y. Kang, H.F. Shen, B. Ding, Arc erosion behavior of a nanocomposite W-Cu electrical contact material, Rare Met. 25 (2006) 37-42.
[24]E. Hantzsche. Mysteries of the Arc Cathode Spot: A Retrospective Glance. IEEE Transactions on Plasma SCIENCE. 2003(31), 799-808.
[25]Y. Feng, T. Bo, H.L. Wang, et.al. Influence of nanocrystallization of CuCr25 on spot diffusion of cathode by vacuum arc, Rare Metal. Mat. Eng. 36 (5) (2007) 929-932.
[26]YP. Wang, C.Y. Zhang, H. Zhang, et.al. Effect of the microstructure of electrode materials on arc cathode spot dynamics. J. Phys. D: Appl. Phys. 36 (2003) 2649-2654.
[27]H.D. Fu, S. Xu, W. Li, et.al. Effect of rolling and aging processes on microstructure and properties of Cu-Cr-Zr alloy. Mater. Sci. Eng. A. 700 (2017) 107-115.
[28]H. Fleiter, J. Weissmuller, O. Wollersheim, R. Würschum. Nanocrystalline materials: a way to solids with tunable electronic structures and properties? Acta Mater. 49 (2001) 737-745.

[29]J.B. Liu, M.L. Hou, H.Y Yang, et.al. In-situ TEM study of the dynamic interactions between dislocations and precipitates in a Cu-Cr-Zr alloy. J. Alloys Compd. 765(2018) 560-568.